Chaotic Solitary Wavelets in 45nm CMOS Adaptive Bias Controlled Ring Oscillators

Sai Venkatesh Balasubramanian

Sree Sai Vidhya Mandhir, Mallasandra, Bengaluru-560109, Karnataka, India.
saivenkateshbalasubramanian@gmail.com

Abstract

A novel kind of iterative map, the frequency dependent map, offering the crucial advantages of easy tunability and signal dependent control is formulated from the standard circle map, and is studied using the bifurcation and cobweb plots. Following this, the nonlinearity of a MOSFET is explored and a novel modification to a conventional ring oscillator is proposed by adding a potential divider in its feedback path, achieving adaptive bias control. It is seen that such a design gives outputs most closely resembling hyperbolic secant based solitons. The ring oscillators, nonlinearly coupled to a 'split-gate' CMOS inverter is seen to generate chaotic signals, which are characterized using standard measures such as phase portrait, Kolmogorov Entropy and Lyapunov Exponent, following which the effect of number of ring oscillator stages on the nature if generated chaos is studied. Finally, the chaotic signal is merged with a hyperbolic secant pulse to form a 'chaotic solitary wavelet', which is seen to possess a high number of vanishing moments with a distinct and unique negative logarithmic slope, a very desirable quality in wavelets, leading to applications such as secure communications, image compression and efficient detection of burst-type signals.

Keywords: Frequency Dependent Chaos, Ring Oscillator, Adaptive Bias Control, Electrical Solitons, Wavelet

1. Introduction

The recent rapid advancement of computer based simulation and data processing technologies have ushered in a new era in physics, an era characterized by systems essentially simple in design, yet giving rise to the evolution of complex patterns over time [1, 2]. This is the very essence of Chaos Theory, which has found application in fields as diverse as astrophysics, biology and engineering [3, 4, 5, 6]. On the electronics front, significant discoveries such as the Chua Circuit have enabled the generation, taming and control of chaotic signals and systems at an unprecedented rate [5]. This has consequently led to a diverse range of applications in the information technology domain such as secure communications, pseudorandom number generators, spatiotemporal patterns and so on [7, 8].

It is well known that the most essential requirement to generate chaos is an iterative map, which specifies how nonlinearities and memory influence the temporal evolution of a system [3, 4]. In this connection, numerous iterative maps have been proposed, examples of which include the logistic map and the standard circle map [3, 4]. Typically, these maps are translated into nonlinear differential equations, which are the implemented at a circuit level using operational amplifiers and passive RLC components [5]. Moreover, other approaches to generating chaos also exist, the most interesting of which involves two ring oscillators coupled with a nonlinear circuit to generate chaos [9, 10, 11, 12, 13, 14].

The present work purports to providing a fresh perspective on electrical chaos generation. Specifically, in stark contrast to the earlier works where the chaotic parameter is usually amplitude or phase, the present work employs frequency as the chaotic parameter. In order to achieve this, the standard circle map, which is an iterative map describing the chaos generated due to two competing driving frequencies, is taken as the basis, and slight modifications and normalizations are performed to modify the circle map into a frequency map [15, 16, 17, 18, 19]. The advantages of employing a frequency dependent chaos are the easy signal dependent control and circuit simplicity leading to ease of implementation. It is observed that the obtained frequency map contains of essentially three components - a switching function, the duo of competing frequencies and the driving signal waveform. This configuration is translated into physical implementation by using two ring oscillators with varying number of stages for the driving signals, and by using the two gate terminals of a 'split gate' CMOS inverter as the nonlinear coupling and switching element. In addition to the conventional ring oscillator design, the present work also explores the 'adaptive bias controlled ring oscillators' formed by inserting a potential divider in the feedback 'ring'. The obtained output signal is characterized and presence of chaos is ascertained using standard measures such as the phase portrait, Lyapunov Exponents and Kolmogorov Entropy [1, 3, 4, 8, 20, 21]. Additionally, the effect of varying the number of ring oscillator stages on the nature of chaos is also explored.

Following this, a novel application involving the generated chaotic signal is proposed - the Chaotic Solitary Wavelet. From a signal processing viewpoint, it has been seen that the wavelet, defined as a compact signal emerges as a very effective tool in the analysis of diverse kinds of real-time data such as Electro Cardio Gram (ECG) and share revenue, as well as in other applications such as image compression [22, 23, 24, 25, 26, 27, 28, 29, 30, 31, 32, 33]. Also, of late, the feasibility and advantages of employing a wavelet based transform rather than the conventional FFT based transform in communication systems such as Orthogonal Frequency Division Multiplexing (OFDM) have been explored [34, 35]. However, from a mathematical perspective, it is well known that for a wavelet to be efficient in such applications, the higher order moments must vanish towards zero, indicating a smooth and compact structure [22, 23, 24, 28]. It is seen that the chaotic solitary wavelets, formed by merging the generated chaotic signal with a hyperbolic secant pulse does satisfy the criteria, thus making it possible to create, without loss of the compactness property, wavelets that offer high security, with the control parameter acting as a secure key.

The simplicity of the proposed chaos generator circuit, coupled with the frequency dependent properties and signal based tuning and the extreme compactness of the chaotic solitary wavelets with maximum number of vanishing moments form the major highlights of the present work.

2. The Circle Map and Frequency Dependent Chaos

The backbone of the present work is the concept of frequency dependent chaos, which gives the advantages of easy tunability and a signal based control. Here, the chaotic parameter is frequency, and the control parameter is the ratio of frequencies between two driving signals. It has been well established in literature that an iterative map ideally suited to describing the nonlinear interactions between two oscillating systems with competing frequencies is the standard circle map [15, 16, 17, 18, 19]. Hence, the 'frequency map' employed in the present work is adapted from the standard circle map, whose iterative map is given as follows [15, 16]:

$$\theta(i+1) = mod(\theta(i) + \Omega + \frac{K}{2\pi} Sin(2\pi\theta(i)), 1) \tag{1}$$

with θ being taken as modulo 1, and K and Ω being the control parameters. The standard circle map represents an area preserving chaotic map physically seen in systems such as the kicked rotator [17, 18, 19].

The key elements of interest in the circle map are the variables θ, the angular phase normalized to unity and Ω, representing an angular frequency factor. Viewing this equation as a purely mathematical relation, as a first step, θ is written as $f_o t$ where f_o represents the normalized version of the angular frequency, given in the units of radians/sample, with a full scale range of $-\pi$ to π.

Also, the time factor t is set to one, representing one sample duration, between the ith and $i+1$th instants. The additive parameter Ω is rewritten as r where $r{=}f_2/f_1$ is the ratio between two normalized competing driving frequencies f_1 and f_2 and is the principal control parameter for the present work. The value of K is arbitrarily set to -2π in order to set the coefficient of the third term of the above equation to unity. Finally, the sinusoid $sin(2\pi\theta(i))$ is viewed as a mathematical function representing the input and is generalised to $V(2\pi f_o(i))$, or alternatively $V(f_o(i))$, with V representing the signal waveform fed to the input of the proposed chaotic system. Using these substitutions, the above equation is rewritten as

$$f_o(i+1) = mod(f_o(i) + r - V(f_o(i)), 1) \tag{2}$$

It is noteworthy that, by making the various modifications to the standard circle map, its physical significance is altered considerably, and it now takes a new form represented by frequency variables and input signal dependence. In order to retain the consistency of the above equation, the various terms are normalized to π. First, the frequency f_o and the frequencies f_1 and f_2 are normalized to the radians/sample scale of $[-\pi, \pi]$. Finally, the term $V(f_o(i))$ is limited to π, i.e. 3.14 Volts by changing the modulus function from 1 to π. The value of 3.14 V, comprehensively encompasses the linear and saturation operating regions of the transistor, as well as forms a convenient normalizing factor yielding effective integration of the frequency and voltage terms. At this point, it is observed that the f and V terms of the above equation are merely reduced to normalized mathematical numbers. Thus, the normalized version of the above equation, with the f and V terms limited to π using a modulus function is given as follows:

$$f_o(i+1) = mod(f_o(i) + \frac{f_2}{f_1} - V(f_o(i)), \pi) \tag{3}$$

This equation is the key iterative map of the present work.

Here the f_o terms denote the output frequencies, whereas f_1 and f_2 denote the frequencies of the input (driving) signals. $V(f_o)$ denotes the input signal waveform employed in the chaotic system. The key elements of the above mentioned iterated function are threefold, enumerated as follows:

1. The modulus function, seen as a switching element and physically realized using the switching operation of a transistor between cutoff and saturation regions [36].
2. The control parameter $r{=}f_2/f_1$ is an additive parameter, and being the key frequency ratio determines when the system transits from order to chaos and vice versa.
3. The $V(f_o)$ introduces a signal dependence, thus enabling the controlling of chaos by changing the waveform used as input.

Based on the above mentioned principles, the bifurcation plot, a plot of f_o as a function of control parameter r is plotted in Fig. (1) for a sinusoidal input between the r values of 1 and 3. From the plot, two key references stand out. First, the bifurcation behavior is periodic, as the pattern repeats after an r interval of 1. Second, it is seen that the control values near integers (1,2,3) and half-integers (1.5,2.5) exhibit significantly lesser 'crowding' suggesting that off-integral values such as irrational ratios give rise to chaos [3, 4].

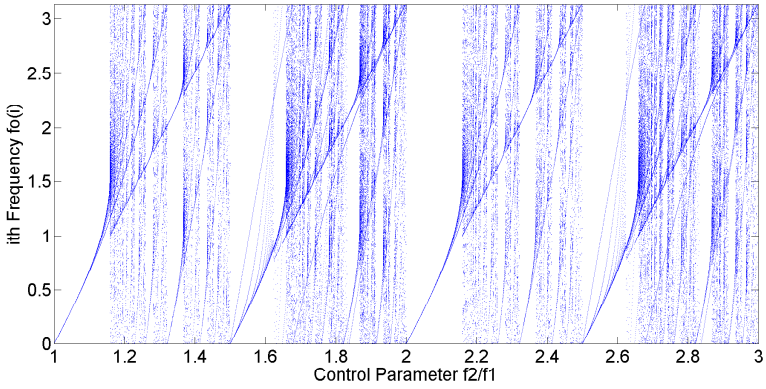

Figure 1: Bifurcation Plot of the Frequency Map with Sinusoidal Driving Inputs

In addition to the bifurcation plot which views f_o as a function of r, another interesting visualization is the Cobweb plot, which shows the evolution of successive iterative samples of f_o for a given value of r. The cobweb plot for a sinusoidal input with an r value of 1.19 is shown in Fig. (2). As is the case with the plot, a well-spread out cobweb plot

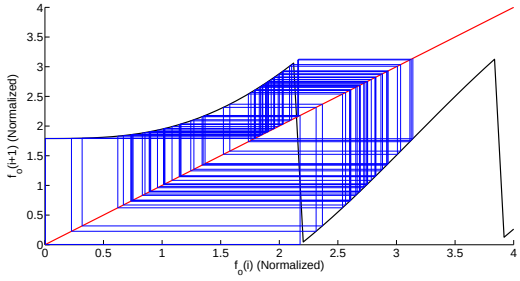

Figure 2: Cobweb Plot of the Frequency Map with Sinusoidal Driving Inputs for an r value of 1.19. Black curve indicates the modulus function whereas blue lines indicate successive evolutions of the iterations of f_o

with mostly non-repetitive patterns suggests a high degree of chaos.

The bifurcation and cobweb plots conclusively describe the chaotic behavior and order-chaos transition of the proposed frequency map.

3. Nonlinear Behavior of a MOS Transistor

The key component in the present work, as is the case in most CMOS technology based designs is the Metal-Oxide Semiconductor Field Effect Transistor (MOSFET) [37, 38, 39]. In the previous section, it had been mentioned that one of the three key elements of the frequency map, namely modulus function could be implemented using the nonlinearity and switching properties of a MOSFET. This nonlinearity primarily is due to the three regions of MOSFET operation (cutoff, linear and saturation) and the transitions between these regions [37, 38]. The nonlinear behavior is best understood by

studying the current-voltage characteristics encompassing both linear and saturation regions, and given by the following expression [40]:

$$I_d = \frac{\mu_n Z C_i}{L}\left[\left(V_G - V_{FB} - 2\psi_f - \frac{V_D}{2}\right)V_D - \frac{2}{3}\frac{\sqrt{2\epsilon j_s q N_a}}{C_i}\left[(V_D + 2\psi_f)^{1.5} - (2\psi_f)^{1.5}\right]\right] \tag{4}$$

In this equation, μ_n denotes the electron mobility, C_i the intrinsic capacitance, V_{FB} is the flat band voltage, j_s is the current density, q is the charge, N_a is the acceptor concentration, ψ_f denotes the work function, L denotes the channel length and Z denotes the channel width, both of which are the key transistor geometry parameters. This nonlinear behavior can be witnessed in the I-V characteristics of a typical NMOS and PMOS transistors sized to $2\lambda \times 4\lambda$ in a 45nm Technology, as shown in Fig. (3) and Fig. (4).

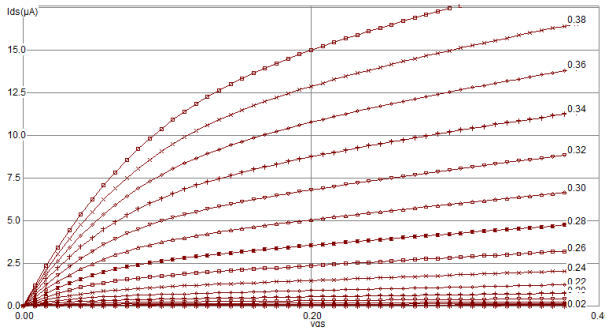

Figure 3: IV Characteristics of a $2\lambda \times 4\lambda$ N-MOSFET in 45nm Technology

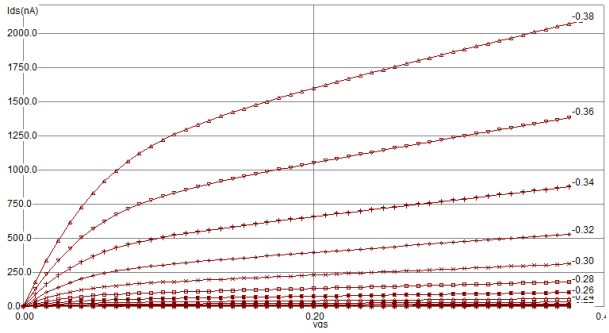

Figure 4: IV Characteristics of a $2\lambda \times 4\lambda$ P-MOSFET in 45nm Technology

Apart from the nonlinearity described above, another significant factor contributing to MOS nonlinearity, particularly at high operating frequencies is the non-quasi static charge model of the MOS channel, which states that the channel of a MOSFET can be modeled as a nonlinear transmission line [41]. An illustration of the NQS model applied to the NMOSFET along with the drain, gate and source capacitances is shown in Fig.(5). Also, the equivalent representation of the nonlinear transmission line is seen as an Elmore resistance, which is length dependent and indicates the effect of wiring and transistor geometry in generation of chaos. The equivalent circuit of Fig.(5), with the Elmore resistance denoted by 'Re' is shown in Fig.(6). The dependance on the Elmore Resistance on the gate-source voltage V_{gs} is given as follows [41]:

$$Re = \frac{L_{eff}}{10\mu_{eff} W_{eff} C_{ox}(V_{gs} - V_{th})} \tag{5}$$

where μ_{eff} is the effective carrier mobility, L_{eff} and W_{eff} denote the effective channel length and width of the NMOS transistor, C_{ox} denotes the oxide layer capacitance and V_{th} is the threshold voltage of the transistor.

The significance of the application of this Elmore Resistance to the Non-Quasi Static model is that the NQS Relaxation time τ depends on a diffusion component $\tau_{diffusion}$ dominant in the subthreshold region of operation, and a drift component τ_{drift} valid in the strong inversion region, with the relation given as follows [41]:

$$\frac{1}{\tau} = \frac{1}{\tau_{diffusion}} + \frac{1}{\tau_{drift}} \tag{6}$$

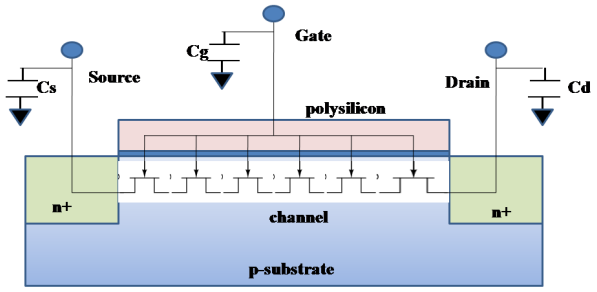

Figure 5: Non-quasi static representation of a NMOS channel

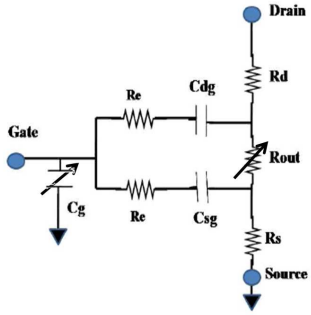

Figure 6: Equivalent circuit of non quasi static channel effect

with the two components of τ given by the following expressions

$$\tau_{diffusion} = \frac{qL_{eff}{}^2}{16\mu_{eff}kT} \tag{7}$$

$$\tau_{drift} = ReC_{ox}W_{eff}L_{eff} \tag{8}$$

with q representing the charge and T representing temperature. The $1/\tau$ based relation is *ipso facto* a frequency oriented relation, and establishes the frequency-oriented charge transport mechanism of the transistor channel [41]. This intuitively suggests how a single transistor can in its natural behavior generate frequency-dependent chaos.

As a direct consequence of the above mentioned factors, an NMOS and PMOS connected to form a CMOS inverter exhibits nonlinear behavior in the transition regions between the usual 'HIGH' and 'LOW' states [36]. This can be understood by observing a transfer curve between the input and output of a single stage CMOS Inverter in 45nm technology and is shown in Fig. (7). The obtained transfer characteristics have been fitted with a sigmoid of the following form, where Vx and Vy represent the Input (Common Gate) and Output side Signals respectively. From the plot, it can be seen that the key nonlinear transition points of the transfer curve lie at around 0.7V and 1V of the input voltage Vx.

$$Vy = 0.0084 + \frac{0.3675}{1 + 10^{-58.8284(0.1595 - Vx)}} \tag{9}$$

4. Ring Oscillator and Adaptive Bias Control

The proposed frequency map in the earlier section details three essential components to generate frequency dependent chaos - switching function, competing frequencies and driving signal waveform. While a 'split gate' CMOS inverter as will be detailed later is used for the switching function, the choice of signal source for competing frequencies in the present work is the ring oscillator. A Ring Oscillator is a resonator-less Oscillator formed by connecting in a closed loop, an odd number of inverters [36]. Since in odd number of inverters, the output of the last stage is a complement of the input to the first stage, this creates a theoretically endless cycle of instability, witnessed by the continuous alternating between low and high states. The time period of the ring oscillator output is given by the relation [36]

$$T = 2MT_d \tag{10}$$

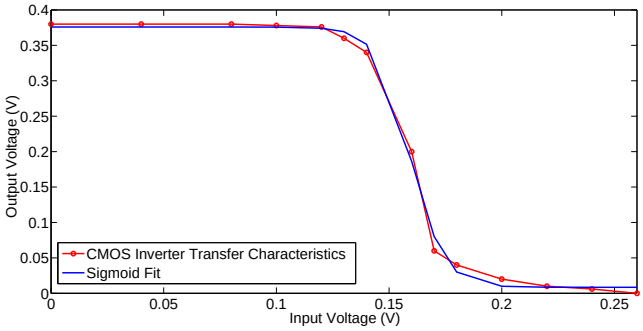

Figure 7: The transfer characteristics of a CMOS Inverter in 45n Technology as obtained from Microwind (red), with a sigmoid fit for the same (blue)

where M denotes the number of stages and T_d is the delay of each stage. Due to this principle, the Ring Oscillator is used as the oscillating element in the proposed design.

All the designs in the present work are implemented at the deep submicron layout level in 45nm CMOS Technology using the Microwind tool [42]. All the NMOS and PMOS transistors are scaled to $2\lambda \times 4\lambda$. This aspect ratio is chosen since it is the smallest for any given technology and as a consequence yields the highest frequencies obtainable.

Thus, in the proposed design, two ring oscillators are chosen as the source of two competing frequencies. Since ring oscillators only contain an odd number of stages, the ring oscillators with the fastest possible output frequencies in any technology are the ones with three and five stages, and these are the configurations used in the present work.

Although the ideal output of a ring oscillator is a never-ending toggle of '0' and '1' states due to the inherent instability, in practice, wiring parasitics and other associated capacitances ensure that the output is seldom a square wave. The nature of a ring oscillator output can be ascertained by examining its spectrum. The FFT spectrum of a 3-stage conventional ring oscillator (shortened as 'RO' for convenience) in 45nm CMOS is shown in Fig. (8). As can be seen, the fundamental frequency is at around 43GHz, with a significant amount of harmonic content.

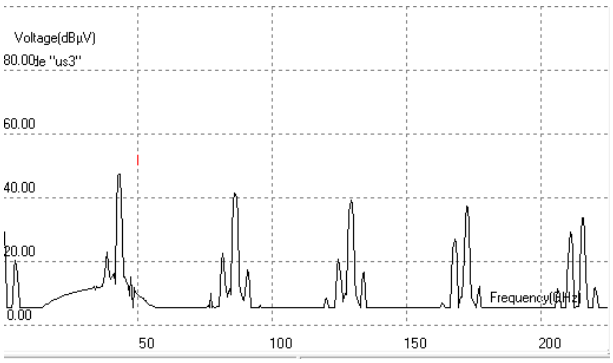

Figure 8: The FFT Spectrum of a 3 Stage Conventional Ring Oscillator

In the present work, a slight modification to the ring oscillator is proposed, that would enable a firm control on the wave shaping and hence the harmonic nature of the output signal. Specifically, a potential divider comprising of two resistors is added in the path between the third inverter output and the first inverter input, as shown in the schematic in Fig. (9).

By setting the value of R1 and R2 to 20kΩ and 100kΩ respectively, the potential dividing factor is set to a value of 0.2. It should be noted at this juncture that the use of a potential divider in the 'ring' enables significant manipulation in the amplitude of oscillation given to the first stage input. This consequently affects the operating point of the first inverter, according to the characteristics shown in Fig. (7). It is for this reason that the proposed design is termed the 'Adaptive Bias Controlled Ring Oscillator', or ABCRO [43, 44, 45]. The FFT Spectra of the ABCRO output is plotted in Fig. (10).

As seen from the plot, one can observe the decrease in the central frequency from 43GHz to 22GHz, while also observing a significant increase in the harmonic content. The exponentially decreasing spectral profile suggests that the ABCRO output might be a train of exponentially shaped pulses. In order to ascertain this, the output voltage waveform of 3 stage ABCRO is plotted and is fitted with a hyperbolic secant based pulse of the ($sech^2$) form in Fig. (11).

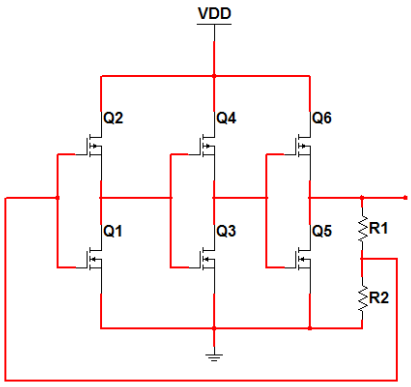

Figure 9: A Three Stage Adaptive Bias Controlled Ring Oscillator

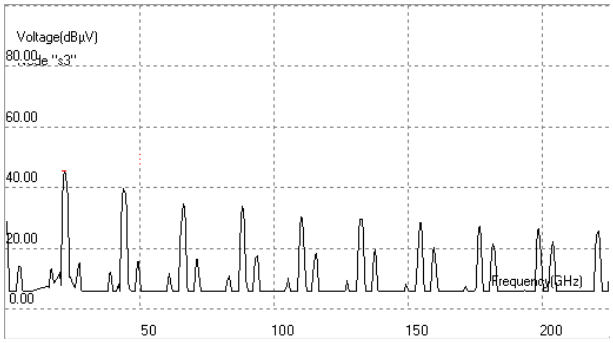

Figure 10: The FFT Spectrum of a 3 Stage Adaptive Bias Controlled Ring Oscillator

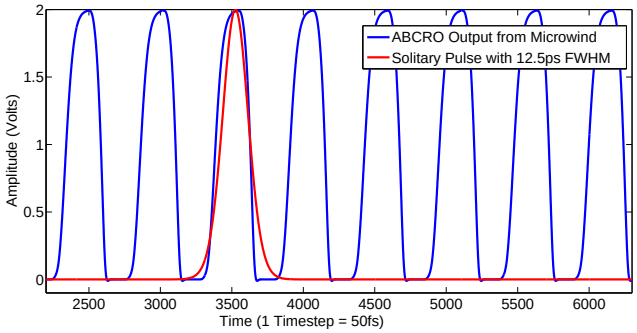

Figure 11: Obtained pulse train from ABCRO, with a single pulse fitted to a hyperbolic secant based solitary pulse ($sech^2$) with a Full-Width Half Maximum (FWHM) at 12.5ps.

It is well known in literature that signals of the form of ($sech^2$) belong to the special class of pulses called the 'Solitons' [46, 47]. Typically, solitons are viewed as mathematical solutions to nonlinear partial differential equations such as the Nonlinear Schrodinger Equation (NLSE), which describe pulse propagation through an optical fiber considering various dispersive and nonlinear effects [46, 47]. A characteristic feature of the Solitary Pulse is its 'bell shape', typically described as a Gaussian or Hyperbolic Secant Function [46, 47]. Also, it has been shown that in prototype Terahertz frequency communication systems such as Radio over Fiber involving both electrical and optical channels, soliton based carriers exhibit significantly lower distortion than the square and sinusoidal counterparts [48, 49].

Thus, it can be seen that the adaptive bias control introduced in the ring oscillator significantly changes the harmonic content of the output waveform, shaping it into a train of solitons, and for this reason, ABCRO's are used as driving frequency sources in the present work.

5. Generation of Frequency Dependent Chaos

Taking cue from the adaptive bias control results of the previous section, a chaos generator circuit is designed. This circuit, whose schematic and layout are shown in Fig. (12) and Fig. (13) respectively, consists of two ring oscillators (ABCRO) with three and five stages and outputs denoted by 's3' and 's5' respectively. These outputs are coupled respectively to the PMOS and NMOS gate inputs of a CMOS inverter whose gate has been 'split'. The asynchronous 'partial' driving of the NMOS and PMOS parts if a CMOS inverter separately, combined with the nonlinearity of a CMOS inverter as seen in Fig. (7), contribute to the generation of chaos using the schematic of Fig. (12), where the CMOS 'split' inverter acts as the physical analogue of the modulus function proposed in the frequency map.

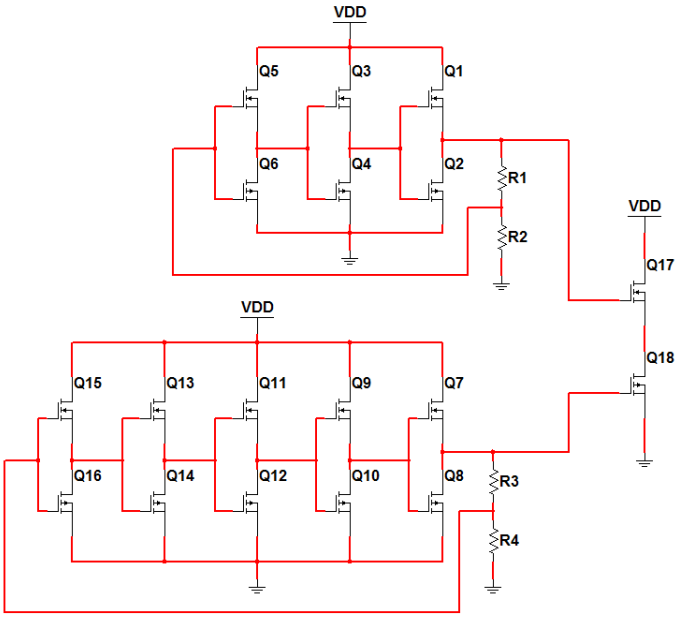

Figure 12: The Schematic of ABCRO based Chaos Generator

The above mentioned layout is implemented in Microwind and the output waveform is shown in Fig. (14). For the purpose of comparison, the output waveform of a chaos generator represented by Fig. (12), but with the ABCRO's replaced with conventional RO's is also shown.

It can be seen from the plots that the ABCRO based chaos output exhibits significant amplitude variations, compared with the conventional counterpart. Also, a general decrease in frequency can be seen, in accordance with the fundamental frequency decrease seen earlier.

6. Characterization of the Generated Chaotic Signal

A Classical Analysis tool for a chaotic signal is its phase portrait. This portrait depicts the time derivative of a signal (dV/dt) as a function of the signal (V) illustrating the dynamics of the signal in the phase space and describing the stability aspects of the chaotic system behavior and points of stability around which the system revolves, qualitatively serving as a tool to assess various chaotic parameters such as sensitivity and ergodicity [3, 4]. The phase plane of the

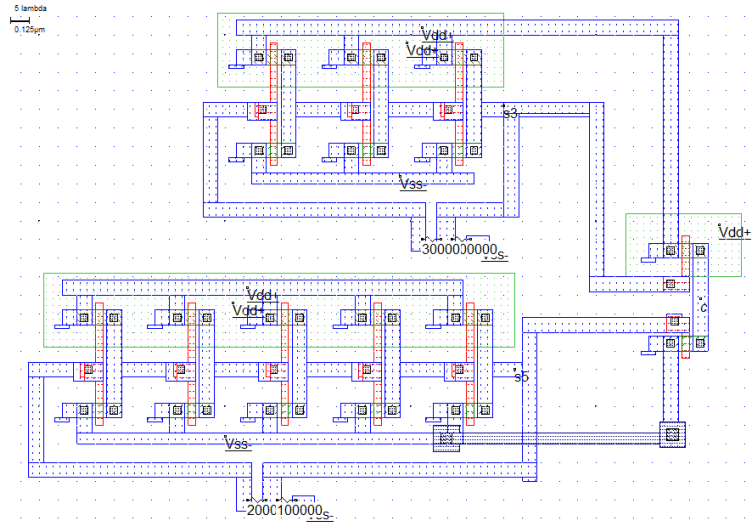

Figure 13: The Layout of ABCRO based Chaos Generator

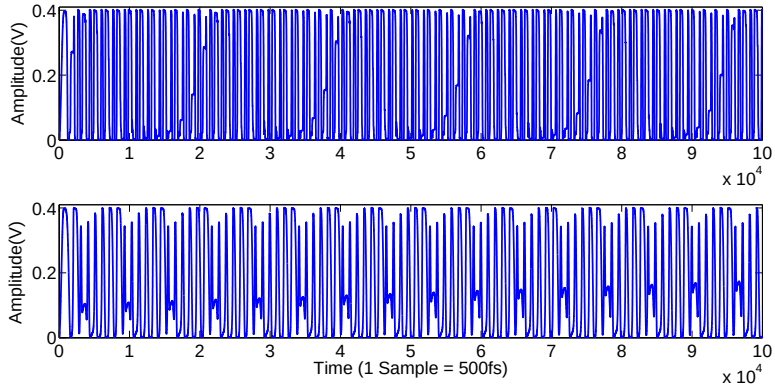

Figure 14: Output Waveform of Chaos Generator circuit using Conventional Ring Oscillators (Top) and Adaptive Bias Controlled Ring Oscillators (Bottom)

generated chaotic signal C is shown in Fig. (15) for both conventional RO and ABCRO cases. From the figure, it is seen that the RO case exhibits an ornamental pattern reminiscent of a quasi-periodic signal breaking into chaos, whereas the ABCRO phase portrait is much more established, displaying certain regions of high sensitivity, such as in the signal value of 0.15.

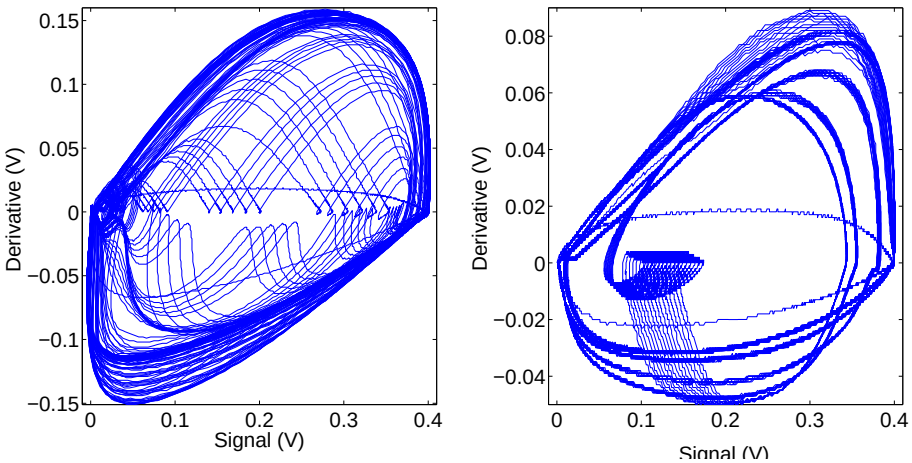

Figure 15: Phase Portrait of the generated chaos output for RO (Left) and ABCRO (Right) Cases

The sensitivity aspect and thus the chaotic nature of the signal C is assertively established by calculating the largest Lyapunov Exponent (LLE), a measure of a system's sensitive dependence on initial conditions [20]. Rosenstein's algorithm is used to compute the Lyapunov Exponents λ_i from the voltage waveform, where the sensitive dependence is characterized by the divergence samples $d_j(i)$ between nearest trajectories represented by j given as follows, C_j being a normalization constant [21]:

$$d_j(i) = C_j e^{\lambda_i (i\delta t)} \tag{11}$$

The Largest Lyapunov exponent thus obtained for the signal C is 4.29, the positive value proving the fact that the signal is indeed chaotic [20].

The suitability of the generated signal as a potential candidate as a carrier for secure communications can be established by ascertaining the amount of information that can be carried by the signal [1, 8, 20]. This is precisely quantified by another standard chaotic characterization measure, the Kolmogorov Entropy, which is essentially a statistical measure of the uncertainty of the signal [8, 20]. By assigning each of the N quantifiable states of the amplitude of C as an event i, the Kolmogorov Entropy K_2 obtained depends on their probabilities p_i according to the relation

$$K_2 = -\sum_{i=1}^{N} p_i \log p_i \tag{12}$$

Since the chaotic output waveform is a continuously varying amplitude, a very high value of N such as 100000 is selected as the number of quantifiable states. Thus, the presence of each of the N states is viewed as an event p_i. The K_2 value thus obtained is 3.63 bits/symbol, clearly testifying to the information carrying capacity of the generated chaotic signal C.

The final aspect of characterization of the generated chaotic signal, is to analyze the effect of number of ring oscillator stages on the nature of the generated chaos. In keeping with the rule of having an odd number of inverters, various combinations of inverter stages including three, five and seven are implemented, and the corresponding parameters of LLE and K_2 are tabulated for both conventional RO and ABCRO cases. From the table, it is observed that the frequency of the driving signals indeed affect the nature of chaos generated.

One interesting observation from the table is that for the Configurations where the ratio r is similar, like for instance in the 5-7 RO and 3-5 ABCRO configurations, the LLE obtained are very similar (4.27 and 4.29 respectively). This establishes the inference that even though the base frequencies and configurations are different for both cases, the nature of the chaos generated is nevertheless very similar owing primarily to the similarity in the r values in the two cases. This indicates that the properties of the chaos generated are primarily determined by the choice of r, the control parameter, as had been initially formulated. Also it can be seen that the general trend of ratio-LLE relationship follows that of the bifurcation plot in Fig. (1), with 'chaotic' ratios such as 1.29 and 1.19 giving much higher LLE values than

Table 1: Effect of Driving Signal Frequency on the Generated Chaos

Type	Stages of A	Stages of B	f_2 (GHz)	f_1 (GHz)	Ratio r	LLE	K_2 (bits/sym)
RO	3	5	43.01	33.3	1.29	4.01	3.64
ABCRO	3	5	22.02	18.4	1.19	4.29	3.63
RO	3	7	43.01	27.8	1.55	0.66	3.64
ABCRO	3	7	22.02	13.6	1.62	2.12	3.64
RO	5	7	33.3	27.8	1.19	4.27	3.63
ABCRO	5	7	18.4	13.6	1.34	3.89	3.63

non-chaotic ratios such as 1.55 and 1.62. This is assertive proof that the proposed frequency map does indeed describe the chaotic behavior of a nonlinearly coupled system of ring oscillators. A detailed and comprehensive derivation of the exact relation between the IV characteristics and the frequency map requires a thorough investigation into multiple aspects of transistor device physics and is a priority for future work [40].

7. Formulation of the Chaotic Solitary Wavelet

As outlined earlier, it is well known that wavelets occupy a crucial niche in signal processing applications, and the addition of security component induced by chaos would certainly provide an additional strength to such wavelets. The formulation of the Chaotic Solitary Wavelet is described as follows, with generated chaotic signal C referring to the signal of the ABCRO case in Fig. (14) [22, 23, 24, 25, 26].

The first step is to define the Scaling Function, also called the 'Father Wavelet' ϕ in continuous time. ϕ is defined as the mathematical product of a hyperbolic secant $sech(t)$ and the generated chaotic signal C. i.e. $\phi(t) = C \times sech(t)$. The choice of hyperbolic secant is dictated by the fact that hyperbolic secant solitons are known to be very smooth, compact functions, making them ideal choices for a wavelet.

The Chaotic Solitary Father Wavelet ϕ thus defined is used as the basis to form the Chaotic Solitary 'Mother Wavelet' ψ, such that the following criteria are satisfied

1. $\psi(t)$ belongs to a subspace of the space $L^1(\Re) \bigcap L^2(\Re)$, the space of absolutely and square integrable measurable functions.
2. $\phi(t)$ and $\psi(t)$ are orthogonal to each other.
3. $\psi(t)$ has zero mean, i.e. the following holds:

$$\int_{-\infty}^{\infty} \psi(t)dt = 0 \tag{13}$$

4. $\psi(t)$ has unity square norm, as per the following equation:

$$\int_{-\infty}^{\infty} |\psi(t)|^2 dt = 0 \tag{14}$$

5. It is preferable, but not a mandatory criterion to ensure that $\psi(t)$ possesses a higher number M vanishing moments. In other words, for all $m < M$,

$$\int_{-\infty}^{\infty} t^m \psi(t)dt = 0 \tag{15}$$

The Chaotic Solitary Mother Wavelet ψ is used to define the solitary daughter wavelets $\psi_{a,b}(t)$ in the following fashion with $a > 0$ denoting the 'scale' and $b \epsilon \Re$ denoting the shift:

$$\psi_{a,b}(t) = \frac{1}{\sqrt{a}} \psi \left(\frac{t-b}{a} \right) \tag{16}$$

The Father, Mother and Daughter Solitary Wavelets are then expressed as discrete signals $\phi(n)$, $\psi(n)$ and $\psi_{a,b}(n)$ centered around zero.

Based on the above procedure, the chaotic solitary father and mother wavelets have been formed using the MATLAB Wavelet Toolbox [29]. The Father and Mother Wavelet Signals are plotted in Fig. (16).

Physically, the existence of vanishing higher moments signifies that the wavelet has a compact, continuous, smooth structure, and that the analysis of bursts in signals with such wavelets can be carried out with minimal filtering [22, 23, 25, 28]. In order to investigate and characterize the performance of the chaotic solitary wavelet, the moments upto

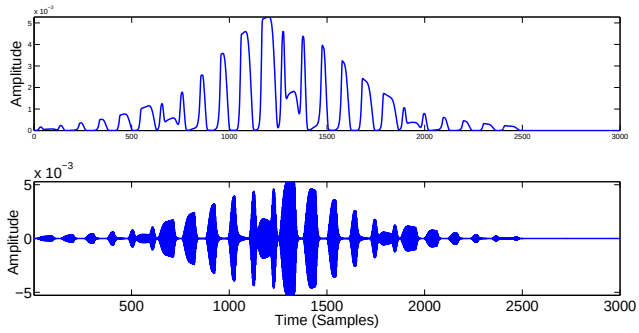

Figure 16: Father and Mother Signals of the Chaotic Solitary Wavelet

Table 2: Moments of Various Wavelets upto the Tenth Order

Moments	DB4	BIOR4.4	RBIO4.4	SYM4	COIF4	DMEY	CSW
First	0.00E+00	0.00E+00	0.00E+00	0.00E+00	0.00E+00	0.00E+00	0.00E+00
Second	1.33E-01	1.09E-01	1.16E-01	1.33E-01	4.26E-02	9.90E-03	5.00E-03
Third	2.05E-02	5.41E-02	8.01E-02	6.96E-02	1.96E-02	3.30E-03	1.60E-03
Fourth	1.13E-01	9.95E-02	1.27E-01	1.30E-01	3.74E-02	7.60E-03	4.80E-04
Fifth	3.25E-02	8.78E-02	1.37E-01	1.14E-01	3.19E-02	5.40E-03	4.00E-04
Sixth	1.05E-01	1.12E-01	1.73E-01	1.52E-01	4.10E-02	7.30E-03	2.00E-04
Seventh	4.19E-02	1.16E-01	2.05E-01	1.58E-01	4.19E-02	6.60E-03	1.67E-04
Eighth	9.95E-02	3.45E-01	2.49E-01	1.90E-01	4.85E-02	7.60E-03	8.00E-05
Ninth	4.96E-02	1.47E-01	2.99E-01	2.08E-01	5.24E-02	7.60E-03	6.00E-05
Tenth	9.56E-02	1.66E-01	3.62E-01	2.42E-01	5.87E-02	8.30E-03	4.00E-05

the tenth order of the chaotic solitary mother wavelet (CSW) are computed and compared with the corresponding moments of six established wavelets, namely Daubechies 4 (DB4), Biorthogonal 4.4 (BIOR4.4), Reverse Biorthogonal 4.4 (RBIO4.4), Symlet 4 (SYM4), Coiflet 4 (COIF4) and the Discrete Meyer Wavelet (DMEY) [29]. The moments are tabulated in Table 2.

From Table 1, it is seen that the higher moments of the chaotic solitary wavelet tend toward zero. It is seen that even in the Meyer wavelet, known to exhibit vanishing moments up to very large orders, moments increase after a certain order (sixth). In order to better capture the trends of the higher moments, the moments of the various wavelets from the third order onwards are plotted on a logarithmic scale in Fig. (17). It is clearly seen that while all the other wavelet

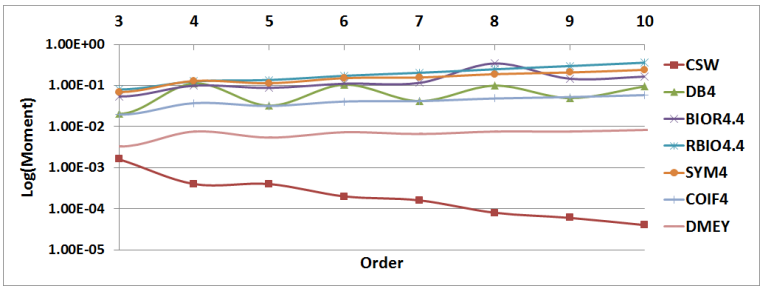

Figure 17: The Moments (upto Tenth Order) of Chaotic Solitary Wavelets compared with contemporary wavelets on a logarithmic scale. The negative slope vanishing fast towards zero clearly sets apart the chaotic solitary wavelet

moments including those of the Dauechies and Meyer show an increasing trend, the chaotic solitary wavelet moments show a decreasing trend with a negative logarithmic slope. This indicates that the moments of the solitary wavelet rapidly decay and vanish toward zero. This gives the chaotic solitary wavelet the exclusive advantages of smoothness, compactness along with the inherent security of the frequency dependent chaos with the control parameter r acting as the secure key.

The formulated chaotic solitary wavelet finds applications of the following three categories:

1. Wavelet Analysis: Since the chaotic solitary wavelet, by virtue of its extremely smooth and compact structure has

a high number of vanishing moments, this wavelet can be used as an efficient way of detecting burst type signals such as ECG, share revenue etc with minimal to no filtering required [30, 31, 32, 33]. Since the formulation of the Father Wavelet involves multiplying the Chaotic signal with a hyperbolic secant, this can be achieved in hardware using a conventional Amplitude Modulator or Mixer based circuit [34]. Given the minimal filtering requirements, this leads to a real-time wavelet analysis technique built using hardware, saving time and power.

2. Signal Processing: The Chaotic Solitary Wavelet can be used in signal and image processing applications such as compression [50]. The added advantage of security implies that this technique can act as a dual purpose compression-encryption scheme for secure informatics.
3. Secure Communications: By replacing the FFT transform block in a conventional system with a Wavelet transform block, a more robust communication system with an additional layer of security can be designed [34, 35].

8. Conclusion

By adapting the standard circle map with slight modifications and normalizations, a frequency map is created, and the properties of this iterative map is studied using bifurcation and cobweb plots. It is seen that the frequency maps give a new perspective into chaos generation by offering the key advantages of easy tunability and signal dependent control. The nonlinearity of a MOSFET is explored in the context of ring oscillators, and it is seen that by adding a simple potential divider in the feedback path, an adaptive bias controlled ring oscillator (ABCRO) is obtained. The output of ABCRO is found to match closely with hyperbolic secant based solitons. Using these inferences, two ABCRO's with three and five stages are nonlinearly coupled to the gates of a 'split inverter' to generate chaos. The generated signal is characterized by Phase portrait, Kolmogorov Entropy and Lyapunov Exponents, and the presence of chaos is indeed ascertained by these analyses. The effect of number of stages on the generated chaos is studied. Finally, the generated signal is merged with a hyperbolic secant pu;se to form a Chaotic Solitary Wavelet. From the analysis of the signal moments, it is inferred that these wavelets have a high number of vanishing moments, tending to zero with a distinct and unique negative logarithmic slope.

Further work in this context would be to examine the relation between the frequency map and MOS IV characteristics, along with trying alternate configurations for the chaos generator, such as an RC potential divider and a heterogenous RO-ABCRO coupling. Finally, the chaotic solitary wavelet could be put to use in various applications as mentioned in the above section.

The simplicity of circuit in generating chaos, coupled with the tunability and signal based control offered by frequency dependent chaos, and the high number of vanishing moments from the chaotic solitary wavelet form the major highlights of the present work.

References

[1] G. B. Giannakis, F. Bach, R. Cendrillon, M. Mahoney, J. Neville. Signal Processing for Big Data, IEEE Signal Processing Magazine, 31, 15 (2014).
[2] M. Hilbert. How much of the global information and communication explosion is driven by more, and how much by better technology?, Wiley Journal of the Association for Information Science and Technology, 65, 856 (2014).
[3] M. Ausloos, M. Dirickx. The Logistic Map and the Route to Chaos: From the Beginnings to Modern Applications, Springer, US, (2006).
[4] S. H. Strogatz. Nonlinear Dynamics and Chaos: With Applications to Physics, Biology, Chemistry, and Engineering ,Westview Press, Cambridge, (2008).
[5] E.Bilotta and P.Pantano. A gallery of Chua attractors, World Scientific, Singapore, (2008).
[6] M. H. Jensen, P. Bak, T. Bohr. Complete Devil's Staircase, Fractal Dimension, and Universality of Mode- Locking Structure in the Circle Map, Phys. Rev. Lett. 50, 1637 (1983).
[7] M. F. Barnsley, A. D. Sloan. Chaotic Compression, Computer Graphics World, 3 (1987).
[8] K. E. Barner and G. R. Arce. Nonlinear Signal and Image Processing: Theory, Methods, and Applications, CRC Press, U.S, (2003).
[9] I. Cicek, G. Dundar. A hardware efficient chaotic ring oscillator based true random number generator, IEEE ICECS, 18, 430 (2011).
[10] I. Cicek, G. Dundar. A chaos based integrated jitter booster circuit for true random number generators, ECCTD, 1, 8 (2013).
[11] Y. Nishio, A. Ushida. Spatio-temporal chaos in simple coupled chaotic circuits, IEEE Trans. Circuits and Systems 1, 42, 678, (1995).
[12] Y. Hosokawa, Y. Nishio, A. Ushida. Chaotic Circuit Using Two Simple Ring Oscillators Coupled by Diodes, Proc. NOLTA, 99, 107, (1999).
[13] Y. Hosokawa, Y. Nishio, A. Ushida. Analysis of Chaotic Phenomena in Two RC Phase Shift Oscillators Coupled by a Diode, IEICE Transactions on Fundamentals, E84-A, 2288, (2001).
[14] Y. Hosokawa, Y. Nishio. Simple Chaotic Circuit using CMOS Ring Oscillators, Int. J. Bifurcation Chaos, 14, 2513, (2004).
[15] R. Gilmore and M. Lefranc. The Topology of Chaos, Wiley,US, (2002).
[16] J. M. T. Thompson and H. B. Stewart. Nonlinear Dynamics and Chaos, Wiley,UK, (2002).
[17] V. I. Arnold. Small Denominators I. Mappings of the circumference onto itself, Am. Math. Soc. Transl, 46, 213 (1965).
[18] M. R. Hermann. Mesure de Lebesgue et nobre de rotation (Geometry and Topology), Springer,Germany, (1977).
[19] R. S. Mackay and C. Tresser. Some flesh on the skeleton: the bifurcation structure of bimodal maps, J. Phys. Lett., 45, L741-L746 (1984).

[20] R. G. James, K. Burke, J. P. Crutchfield. Chaos forgets and remembers: Measuring information creation, destruction, and storage, Int. J Bifurcation Chaos. 378, 2124 (2014).
[21] M. T. Rosenstein, J. J. Collins, C. J. De Luca. A practical method for calculating largest Lyapunov exponents from small data sets, Physica D, 65, 117, (1993).
[22] D. R. Larson. Wavelet Analysis and Applications, Birkhuser, (2007).
[23] D.J.Greenhoe. Wavelet Structure and Design, Abstract Space Publishing,(2013).
[24] A.Jensen and A.C.Harbo. Ripples in Mathematics: The Discrete Wavelet Transform, Springer, (2001).
[25] H.Fuhr. Abstract Harmonic Analysis of Continuous Wavelet Transforms, Springer, (2005).
[26] T.Cooklev. An efficient architecture for orthogonal wavelet transforms, IEEE Signal Processing Letters, (2006), 13, 77.
[27] A.N.Akansu and R.A.Haddad. Multiresolution Signal Decomposition, Academic Press, (2001).
[28] I.Daubechies. Different Perspectives on Wavelets, American Mathematical Society, (1993).
[29] M.Weeks. Digital Signal Processing using MATLAB and Wavelets, Jones and Bartlett, (2011).
[30] A.Gacek and W.Pedrycz. ECG Signal Processing, Classification and Interpretation, Springer, (2011).
[31] D.Rosenbaum. Quantitative Cardiac Electrophysiology, CRC Press, (2002).
[32] S. Turner, M. C. Feurstein and M. C. Teich. Multiresolution Wavelet Analysis of Heartbeat Intervals Discriminates Healthy Patients from Those with Cardiac Pathology, Physical Review Letters, (1998), 80, 1544.
[33] R.Schabacker. Technical Analysis and Stock Market Profits, Harriman House Ltd.,(2005).
[34] B.Sklar, Digital Communications: Fundamentals and Applications, Pearson, California, (2010).
[35] L. L. Scott, M. K. Ibrahim, M. M. Al-Akaidi. Orthogonal wavelet division multiplex: an alternative to OFDM, IEEE Trans. Consumer Electronics, 53, 278 (2007).
[36] B. Razavi, RF Microelectronics, Prentice Hall, US, (2011).
[37] F. Balestra, Nanoscale CMOS: Innovative Materials, Modeling and Characterization Wiley,US, (2013).
[38] I.Ferain, C.A.Colinge and J.P.Colinge. Multigate transistors as the future of classical metal oxide semiconductor field effect transistors. Nature, 479, 310 (2011).
[39] D.Lizzit, P.Palestri, D.Esseni, A.Revelant and L.Selmi. Analysis of the Performance of n-Type FinFETs With Strained SiGe Channel. IEEE Transactions on Electron Devices. 60, 1884 (2013).
[40] B. G. Streetman and S. K.Banerjee, Solid State Electronic Devices, PHI, U.S, (2006).
[41] M.Chan, K.Hui, C.Hu and P.K.Ko. A robust and physical BSIM3 non quasi static transient and AC small signal model for circuit simulation. IEEE Transactions on Electron Devices. 45, 834 (1998).
[42] J.P.Uyemura. Chip Design for Submicron VLSI: CMOS Layout and Simulation. USA: Thomson/Nelson, (2006).
[43] D. Ricketts, X. Li, and D. Ham. Electrical soliton oscillator, IEEE Trans. Microwave Theory and Techniques 54 , 373, (2006).
[44] D. Ham, X. Li, S. Denenberg, T. H. Lee and D. S. Ricketts. Ordered and chaotic electrical solitons: communication perspectives, IEEE Communications Magazine 44 , 126, (2006).
[45] O. O. Yildirim, D. S. Ricketts and D. Ham. Reflection soliton oscillator, IEEE Trans. Microwave Theory and Technique 57 , 2344 (2009).
[46] Y.S.Kivshar and G.Agrawal. Optical Solitons: From Fibers to Photonic Crystals. USA: Academic Press (2013).
[47] K. Porsezian, R. Ganapathy, A. Hasegawa and V. N. Serkin. Nonautonomous Soliton Dispersion Management, IEEE Quantum Electronics, 45, 1577, (2009).
[48] R. Ganapathy, M. Easwaran, G. J. Raj, B. Sai Venkatesh and K. Porsezian, Modeling and evaluation of Radio over Fiber Communication Systems on employing Nanophotonic Devices, ICONSET, 181, (2011).
[49] B. Sai Venkatesh, R. Ganapathy and K. Porsezian, Design of Terahertz Radio over Fiber - Beyond 4G, WRAP, (2013).
[50] D.S. Cruz, C. Ebrahimi, J. Askelof, M. Laarsson, C. A. Chritsopoulos, JPEG 2000 still image coding versus other standards, SPIE Digital Image Processing XXIII, 4115, 446 (2000).